P. Chando International Journal of Applied Pharmaceutics

ISSN- 0975-7058 Vol 18, Issue 4, 2026

Original Article

INVESTIGATION OF PHYSICOCHEMICAL STABILITY AND ANTI-PSORIATIC EFFICACY OF LAVENDER OIL NANOEMULSION IN PSORIATIC HACAT CELLS

PURVA CHANDORKAR, SWATI JAGDALE*

School of Health Sciences and Technology, Department of Pharmaceutical Sciences, Dr. Vishwanath Karad MIT World Peace University, Kothrud-411038, Pune, MH, India

***Corresponding author: Swati Jagdale; *Email: swati.jagdale@mitwpu.edu.in**

Received: 09 Mar 2026, Revised and Accepted: 20 May 2026

ABSTRACT

Objective: The objective of this research was to develop a nanoemulsion of lavender oil (LO) and evaluate its physicochemical properties. The effects of LO relevant to psoriasis were also determined on stimulated human keratinocyte (HaCaT) cells by evaluating its cytotoxicity, anti-microbial potential, and alterations in the levels of pro-inflammatory markers.

Methods: A stable LO-based nanoemulsion was developed using a pseudo-ternary phase diagram approach, employing Tween 80 (T80) and Transcutol P (Tp) in a 2:1 ratio. The optimized formulation exhibited a particle size (PS) of 98.91±1.02 nm, zeta potential (ZP) of −11±0.98, and a polydispersity index (PDI) of 0.174±0.001. The formulation was evaluated for anti-oxidant and antimicrobial activity, cytotoxicity against stimulated HaCaT cells and its effect on pro-inflammatory cytokine expression.

Results: The developed LO nanoemulsion demonstrated measurable radical scavenging activity and a weak antimicrobial effect against *Staphylococcus aureus*. Batch A3 showed high cytotoxicity in stimulated HaCaT cells with an IC_{50} value of 0.4198±0.047 µl**/ml, compared to 7.843±0.029 µl**/ml for dithranol. Additionally, the formulation reduced the expression of interleukin-17 (IL-17) by 10% and interleukin-22 (IL-22) by 29%.

Conclusion: The findings indicate that the LO nanoemulsion exhibits *in vitro* anti-inflammatory and cytotoxic effects relevant to psoriatic conditions, including oxidative stress, microbial activity, and inflammatory mediators. However, these observations are based on *in vitro* findings and should be interpreted as preliminary. Further in-depth *in vivo* and clinical investigations are required to establish its therapeutic relevance.

Keywords: HaCaT, IL-17, IL-22, Lavender oil, Nanoemulsion, Psoriasis

DOI: https://dx.doi.org/10.22159/ijap.2026v18i4.58875 Journal homepage: https://innovareacademics.in/journals/index.php/ijap

INTRODUCTION

Psoriasis is a self-amplifying immune system disorder, responsible for chronic skin inflammation, affecting approximately 2-3% of the global population, and 0.51% of children all round. It is characterized by hyperproliferation of keratinocytes, abnormal differentiation of the epidermis and excessive inflammatory manifestation that clinically displays as erythematous, scaly plaques on the head (scalp), knees, elbows, and the lower back. It significantly impacts quality of life, and in extreme situations, the disease could be accompanied by comorbidities in the form of psoriatic arthritis, heart complications, as well as mental strain [1, 2]. Psoriasis pathophysiology is complex and includes factors of hereditary tendency, environmental aspects (e. g., stress, infection, trauma), and the immune system imbalance. Activation of T-helper (Th1/Th2/Th17) immune pathways plays a central role in disease progression and increases the expression of proinflammatory cytokines. The Th17 type of helper T-cells are majorly responsible for the synthesis of interleukin-17 (IL-17) and interleukin-22 (IL-22) [3, 4]. When IL-17 reaches the keratinocytes, proinflammatory facilitators such as cytokines (TNF-α, IL-6), chemokines (CXCL1, CCL20) and antimicrobial peptides (β-defensins) are produced, which recruit excessive immune cells into the skin to maintain chronic inflammation. Whereas, in the case of IL-22, keratinocyte hyperproliferation takes place and the epidermal cell differentiation is inhibited, leading to acanthosis and abnormal epidermis. This simultaneous action of IL-17-mediated inflammation and IL-22-induced epidermal remodelling confirms a self-amplifying loop amongst keratinocytes and immune cells [5–7]. The existing treatment comprising topical corticosteroids, vitamin D analogues, systemic immunomodulators and even the biologics provides symptomatic benefits only, which is associated with adverse effects like skin atrophy, systemic toxicity, and drug efficacy diminution due to long-term usage [8]. This highlights the need to adopt safer, more effective, and skin-targeted treatment strategies, particularly for patients with mild-to-moderate disease.

Lavandula angustifolia, known as lavender oil (LO), is a familiar herbal oil in traditional medication which has a great abundance of bioactive constituents like linalool and linalyl acetate. It has strong anti-inflammatory, antimicrobial, antioxidant, and wound-healing activities. In a study by Narayan P. Yadav *et al.* [9] the effect of both linalool and linalyl acetate, the significant elements of LO showed results in the imiquimod-induced mouse model. Recent studies have demonstrated the anti-inflammatory and anti-oxidant potential, and is therefore potentially a good candidate drug in the levelling out of the immune response in skin disorders like eczema and psoriasis [10, 11]. The major phytoconstituents of LO, particularly linalool and linalyl acetate, are known to modulate several molecular pathways implicated in psoriasis. Linalool has been reported to suppress the excessive production of proinflammatory cytokines, for example, TNF-α, IL-17, and IL-22 by preventing the stimulation of the NF-κβ signalling cascade, thereby reducing keratinocyte hyperproliferation and inflammatory cell infiltration. Similarly, linalyl acetate exhibits antioxidant potential through enhancement of endogenous enzymatic defences like superoxide dismutase and catalase, mitigating oxidative stress that contributes to epidermal damage in psoriatic lesions. These combined effects may help restore epidermal homeostasis and improve barrier function in psoriatic skin [12, 13]. Moreover, it can be used against micro-organisms, which can decrease the possibilities of secondary infections by the lesions of psoriasis [14]. The therapeutic use of LO, however, is hampered by the fact that it has poor water solubility, poor skin permeation, is atmospherically unstable, photosensitive and can be irritating when in concentrated doses [15]. By encapsulating LO in a nanoemulsion system, these limitations could be resolved as it would help to improve its stability, the percutaneous absorption, and controlled release [16]. Although nanoemulsions have been widely investigated for the delivery of both synthetic and herbal actives in various dermatological conditions, their application in psoriasis remains limited, particularly for essential oil-based systems. Specifically, there is a lack of systematic studies evaluating LO-loaded nanoemulsions in the context of psoriasis, despite the well-documented anti-inflammatory and antioxidant properties of its major

constituents. Furthermore, limited information is available regarding the biological response of such formulations in psoriatic keratinocyte models, particularly with respect to key cytokines such as IL-17 and IL-22, which play a central role in disease progression. Therefore, the present study aims to address this gap by developing and evaluating an LO-based nanoemulsion and investigating its effects on cytokine modulation in stimulated HaCaT cells. This approach provides insight into the potential of LO nanoemulsion as a targeted topical strategy for psoriasis management.

The diverse activity of LO and, especially, its anti-inflammatory and antibacterial actions could be used as a topical therapy option in psoriasis that synergistically treats inflammation of immune origin and the microbiome colonization that follows. *In vitro* cell toxicity was evaluated by means of stimulated HaCaT cells to determine the potential of LO nanoemulsion as an anti-psoriatic formulation. The ELISA, specifically for determining the levels of IL-17 and IL-22, was implemented as they are the key cytokines involved in psoriasis. These results can provide an avenue to working out a harmless, herbal and effective topical treatment of the psoriatic lesions. Though the current study focuses on *in vitro* assessments, complementary *in vivo* studies using established models such as imiquimod-induced psoriasis in mice are warranted to validate therapeutic outcomes in a complex immune microenvironment.

MATERIALS AND METHODS

Chemicals and reagents

LO was purchased from Prist Herbochem (Pune, India). Tween 80 (T80), ethanol, methanol, ethyl acetate and pyridine (all analytical grade) were acquired from Loba Chemie (Mumbai, India). Transcutol® P (Tp) was supplied as a gift by Gattefossé India. N, O-bis(trimethylsilyl)-trifluoroacetamide, comprising 1% trimethyl-chlorosilane (BSTFA+TMCS, 99:1), was used as the derivatising agent for GC-MS. Double-distilled water was prepared in-house. Mueller-Hinton Agar (MHA), the standard *Staphylococcus aureus* strain (ATCC 25923), Mueller-Hinton Broth (MHB), and rifampicin (3 µg) discs were from HiMedia Laboratories (Mumbai, India). Cell culture reagents Dulbecco's Modified Eagle Medium (DMEM), Fetal Bovine Serum (FBS), a solution of penicillin-streptomycin and3-(4,5-dimethylthiazol-2-yl)-2,5-diphenyltetrazolium bromide (MTT) were also from HiMedia. Human keratinocytes (HaCaT) were obtained from NCCS, Pune. A commercial GENLISA™ ELISA kit (Krishgen Biosystems, India) was used for IL-17 and IL-22 determination. All remaining chemicals used are analytical grade as supplied. All numerical data are provided using the mean±SD for at least three separate replicates.

HaCaT cell culture and induction of psoriasis-like inflammation

The human keratinocyte (HaCaT) cells were grown at 37 °C in a humidified 5% CO_2 environment using DMEM accompanied with 10% FBS and 1% penicillin-streptomycin. Cells were seeded and allowed to reach 80-85% confluency for each experiment. Following standard induction techniques, 100 ng/ml recombinant IL-17 was used for the treatment of the cells for 24 h to induce psoriasis-like inflammation [17]. After the stimulation period, the medium containing IL-17 was removed, and cells were washed with phosphate buffer solution (PBS). The stimulated cells were then exposed to various concentrations of blank nanoemulsion, batch A3 and dithranol for an additional 24 h for subsequent assays.

Preliminary studies

Gas chromatography-mass spectrometry (GC-MS) of LO

The chemical compositions of the oil were revealed by following the previously reported method with some modifications [18]. Briefly, Shimadzu GCMS-QP2010 (Japan) Ultra system with a 30 m capillary column having 0.25 µm film thickness, inner diameter of 0.25 mm and helium (carrier gas; flow rate of 1.21 ml/min) was utilized. 2 µl** of sample (concentration 50 mg/ml) for semi-quantitation was injected using an autosampler. Injection was done in split mode (split ratio 10:1) at 260 °C. After two min at 120 °C, the oven temperature was raised to 300 °C at an increasing rate of 10 °C/min and was maintained for 20 min. For detection, mass spectroscopy was employed. Prior to analysis, the sample underwent derivatization using BSTFA+TMCS to enhance the volatility of relatively less volatile or polar constituents, enabling their detection during GC-MS analysis and facilitating broader chemical profiling of the oil. 10 µl pyridine was added to the concentrate. The mixture was moved to a 2 ml GC vial, dried with nitrogen gas, and then reconstituted in methanol before analysis.

Fourier transform infrared spectroscopy (FTIR) analysis

FTIR spectra of individual components and its physical mixture were noted in the scanning range of 400-4000 cm^{-1} at room temperature (RT) using Shimadzu QATR-S (Japan) model. The graphs were plotted using OriginPro 2025, learning edition software.

Construction of pseudoternary phase plot

Pseudoternary phase plots were prepared using Ternaryplot. com by water-titration at RT to establish the optimal concentration ranges of constituents for nanoemulsion formation [19]. Initially, T80 was selected and emulsification was observed. Further, various surfactant and co-surfactant (s-mix) combinations, including labrasol-Tp, tween 60-span 80, T80-span 80, and T80-Tp, were evaluated at varying weight ratios of 1:1, 1:2, and 2:1. For every plot, the oil phase and the s-mix were mixed in varying weight ratios (1:9, 2:8….9:1). The water was added dropwise using a micropipette in increments of approximately 10-20 µl** at constant stirring, and the system was visually monitored after each addition until turbidity or phase separation was observed. The transparent region indicated the nanoemulsion region. After dropwise addition of water, the mixture was observed for its clarity and phase separation. The end point of titration was determined as the point where turbidity or phase separation occurred. The concentration ranges of oil and s-mix, along with water, were recorded, and the data obtained is then plotted to get pseudo-ternary phase diagrams. These diagrams guided the selection of appropriate component ratios for further formulation studies.

Formulation of LO nanoemulsion

LO nanoemulsion was prepared using a two-step emulsification process [20]. Initially, s-mix in a ratio of 1:2 was mixed with water to obtain an aqueous phase. A preliminary coarse emulsion was then developed by adding LO, acting as the oil phase, to the water phase and stirring the mixture with a magnetic stirrer at 250 rpm. This coarse emulsion was then processed into a nanoemulsion using a probe sonicator (Sonics Vibra-cell, VCX-750, USA; 3 mm probe diameter). Probe sonication was carried out using a 20 s ON/10 s OFF cycle at 25 °C and the formulation was maintained in a water bath throughout the process to prevent heat generation and possible thermal degradation of LO constituents. Three batches (A1, A2, and A3) with varying oil concentrations were prepared following the same method as mentioned in table 1.

Table 1: Composition of LO nanoemulsion batches A1, A2 and A3

Batch	Oil (%)	S-mix (2:1) (%)	Water (%)
A1	14.45	14	71.12

A2	28.91	16.04	55.05
A3	10.10	13.73	76

Note: S-mix is surfactant/co-surfactant in a ratio of 2:1; all the values are in % v/v.

Characterization of nanoemulsion

Zeta potential and particle size measurement

Zeta potential (ZP), particle size (PS) and polydispersibility index (PDI) of all the batches were determined by means of a Malvern Zetasizer (Nano ZS90, UK) equipped with dynamic light scattering (DLS) technology [21]. So as to ensure through dispersion and avoid particle aggregation, the nanoemulsion was diluted 100× with distilled water at 25 °C.

Thermodynamic stability of nanoemulsion

To determine the stability of prepared nanoemulsion batches (A1, A2, A3) thermodynamic stability study was used [22]. 1) Centrifugation Test: The centrifugation was carried out on the batches at 5000 rpm for 60 min. The samples were then checked for signs of variability such as phase separation, cracking, or creaming. 2) Heating-Cooling Cycles: Six cycles of the temperature variation were repeated, first at 4 °C and then at 40 °C, with the duration of one cycle being 48 h. 3) Freeze-Thaw Cycles: All three batches were placed into the freezer at-25 °C for 24 h. Thereafter, they were stored at RT (25 °C) to determine whether the nanoemulsions transformed back into their original structure without apparent modifications.

Drug content

A UV-VIS spectrophotometer (Shimadzu, UV-1780, Japan) was utilized to quantify the amount of drug in batch A3. To break the nanoemulsion, 1 ml was diluted up toa volume of 10 ml with ethanol in order to guarantee total solubilization of the drug. The blend obtained was mixed magnetically at RT for 30 min to attain a homogeneous mixture. Thereafter, the mixture was analysed at 273 nm to analyse the drug content [23].

Drug release study using the dialysis bag method

In the experiment, the drug release characteristics of batch A3 and pure LO were investigated by means of the dialysis bag method in PBS pH 7.4 [24, 25]. Dialysis membrane 50 (MWCO 12-14 kDa) was first wetted in PBS for 12 h before use. In the dialysis bag, 2 ml of the sample was poured and dipped in 100 ml of the dissolution medium at 37±2 °C with constant stirring at 50 rpm. Samples were taken out of the dissolution medium at certain pre-decided times (0, 1, 2, 3, 4, 5, 6, 7 and 8 h). An equal amount of PBS was substituted after every withdrawal to keep the sink condition. The released drug concentration was quantified spectrophotometrically at 278 nm. Quantification was done based on the standard calibration of LO in PBS. The obtained absorbance was used to calculate cumulative drug release over time.

***In vitro* DPPH radical scavenging assay**

The anti-oxidant effect of LO and A3 was estimated through the 2,2-diphenyl-1-picrylhydrazyl (DPPH) radical scavenging approach, having small changes as compared to an earlier established protocol [26]. A standard solution of ascorbic acid was obtained by dissolving 1g in 10 ml of distilled water. 60 µg/ml mixture of DPPH was obtained by solubilizing 6 mg in 100 ml of methanol. In clean test tubes, 1 ml of each test sample was taken at different levels of concentration and combined with 1 ml of DPPH solution. The resultant solutions were placed in the dark at RT to enable the reaction to take place within a time frame of 20 min. After the incubation time was over, the absorbance of the individual sample was measured spectrophotometrically at 517 nm. As a negative control, a methanolic DPPH solution that did not contain any sample was kept and ascorbic acid was employed as a positive control. The percent of scavenging property was determined via the equation 1.

$$\% \text{ Scavenging Activity } = \frac{\text{Abs}_{\text{control}} - \text{Abs}_{\text{sample}}}{\text{Abs}_{\text{control}}} \times 100 \ldots\ldots\ldots (1)$$

Where, $\text{Abs}_{\text{control}}$ is absorbance of the control and $\text{Abs}_{\text{sample}}$ is absorbance of the sample.

***In vitro* antimicrobial assay**

To evaluate the antibacterial activity of the LO nanoemulsion, the Kirby-Bauer (agar disc diffusion method) technique on MHA plate was used. *S. aureus* was used as the test organism [27]. MHB was used to prepare the bacterial inoculum, which was then standardized to a 0.5 McFarland standard (about 1.5×10^8 CFU/ml). MHA plates were uniformly inoculated by spreading 100 µl** bacterial suspension. Sterile discs with a diameter of 5 mm were impregnated using 10 µl** of the batch A3 at different concentrations (0, 6.25, 12.5, 25, 50 and 100% (v/v)) and placed on the inoculated agar surface. A commercial rifampicin disc (3 µg) was utilized as the positive control, while a disk filled with solvent alone was employed as the vehicle control. To evaluate the zone of inhibition, the plates were subjected to incubation at 37 °C for 24 h, zone was then measured in mm to measure antibacterial activity. The presence and size of the inhibition zone indicated the extent of antimicrobial efficacy of the tested formulation.

Morphological analysis

Following treatment with batch A3, morphological alterations in HaCaT cells were evaluated using brightfield microscopy. The cells were cultured under standard conditions with or without the nanoemulsion for 24 h. After the incubation time, an optical microscope with a high-resolution digital camera was used to analyse the cellular morphology. Images were taken using a 100× objective lens to enable a detailed evaluation of structural alterations in the treated and untreated cells.

Cytotoxicity study

The cytotoxic activity of nanoemulsion batch A3 was estimated by MTT assay [28]. Briefly, stimulated HaCaT cells at a density of 10,000 cells/well were seeded in 96-well plates and kept for 24 h to adhere. Cells were then treated with varying strengths of the blank nanoemulsion, batch A3 and dithranol (226.23 g/mol) prepared from a DMSO stock (0.5%) and diluted in medium without FBS. Untreated cells served as the control, and wells without MTT reagent served as blanks. After 24 h, 20 µl** of 5 mg/ml MTT solution was supplemented to every well and incubated for 2 h. The formazan crystals were solubilized using 100 µl** of DMSO after discarding the supernatant. An ELISA plate reader (iMark, Bio-Rad, USA) was used to assess the absorbance at 540 nm. Cell images were obtained employing an Olympus EK2 inverted microscope (Japan) with a digital camera (AmScope 10 MP). IC_{50} values were analysed using GraphPad Prism 6. Results are stated as mean±SD (n = 4). All concentrations of nanoemulsion are expressed as µl**/ml (v/v) due to the liquid nature of the formulation. As the nanoemulsion is a multicomponent system, direct conversion to mass-based units (µg/ml) was not directly feasible. Dithranol concentrations were prepared in equivalent volumetric units for comparative analysis.

Enzyme-linked immunosorbent assay (ELISA)

The amount of IL-17 and IL-22 was measured in stimulated HaCaT cells using the procedure of the manufacturer. In short, the necessary volume of samples was introduced into the pre-coated wells of the ELISA plate. For IL-17 estimation, the plate was incubated at RT for 2 h, whereas for IL-22 estimation, incubated at 37 °C for 1 h. Then, wells were washed 4 times with 1× (assay diluent) of wash buffer and any leftover liquid was dried by turning the plate upside down and blotting gently on an absorbent material. After that, each well was introduced with a biotin-conjugated solution (100 µl**). The plate was resealed and incubated for 1 h at RT, after which a repetition of the wash was done as mentioned above. Then, 100µl* of diluted combination of Streptavidin-HRP was added to each well and kept for incubation at RT for 1 h. After the final wash, colour change was attained by adding 3,3',5,5'-Tetramethylbenzidine (TMB) substrate solution. For IL-17 estimation, 100 µl** of TMB solution was added after incubation in the dark for 30 min, whereas for IL-22 estimation, equal volumes of substrate solutions A and B (50 µl** each) were added and incubated at 37 °C in the dark for 15 min. Stop solution of 100 µl** was added to end the enzymatic reaction. The readings of optical density were taken on a microplate reader within 30 min after the reaction stopped at 450 nm. Cytokine concentrations were calculated from the respective standard curves.

RESULTS

Preliminary studies

Gas chromatography-mass spectrometry (GC-MS) of LO

GC-MS identified 21 phytoconstituents contributing 100% of the total peak area. Linalyl acetate (27.81%) and linalool (14.87%) were the major components. Other notable constituents included diethyl phthalate (6.43%), 3,5,5-trimethylhexyl acetate (6.48%), and α-terpineol (4.86%). The chromatogram and compound details are given in fig. 1 and table 2.

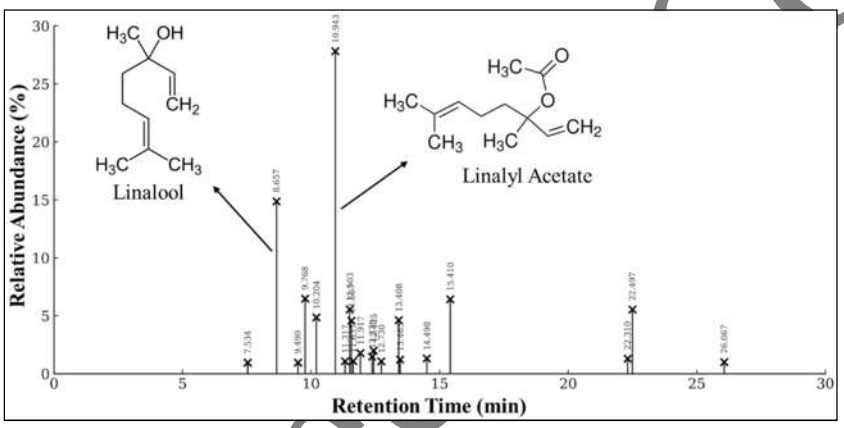

Fig. 1: GC-MS chromatogram of LO indicating presence of linalyl acetate (27.81%) and linalool (14.87%)

Table 2: Major chemical constituents of LO identified by GC-MS

S. No.	Name	Chemical class	% Area
1	Cyclohexene, 1-Methyl-4-(1-Methylethenyl)	Monoterpene hydrocarbon	0.96
2	Linalool	Monoterpene alcohol	14.87
3	α-Terpineol		4.86
4	Bicyclo-[2,2,1]-Heptan-2-One, 1,7,7-Trimethyl-(1S)	Monoterpene ketone	0.96
5	3,5,5-Trimethylhexyl Acetate	Aliphatic ester	6.48
6	Linalyl Acetate	Monoterpene ester	27.81
7	Isobornyl Acetate		4.57
8	α-Terpinyl Acetate		1.47
9	Neryl Acetate		1.07
10	2-Propenal, 3-Phenyl	Aromatic aldehyde	1.07
11	Benzene, 1-Methoxy-4-(1-Propenyl)	Phenylpropanoid ether	5.55
12	Phenol, 2-Methoxy-3-(2-Propenyl)	Phenylpropanoid phenol	3.47
13	Phenol, 2-Methyl-5-(1-Methylethyl)	Phenolic monoterpenoid	1.1
14	1,2-Benzenedicarboxylic Acid, Monomethyl Ester	Phthalate ester	1.78
15	Diethyl Phthalate		6.43
16	1,4-Benzenedicarboxylic Acid, Bis(2-Ethylhexyl)-Ester		1.01
17	Dihydro-Nor-Dicyclo-Penta dienyl Acetate	Bicyclic ester	4.62
18	Bicyclo-[7,2,0]-Undec-4-Ene, 4,11,11-Trimethyl-8-Methylene-[1r-(1r*,4e,9s*)]	Sesquiterpene hydrocarbon	1.23
19	1H-Benzocycloheptene, 2,4a,5,6,7,8-Hexahydro-3,5,5,9-Tetramethyl	Polycyclic aromatic hydrocarbon derivative	1.32
20	2-Fluoromethyl-1,3,6,8-Tetrakis-(2'-Fluoroethyl)-1,3,6,8,10-Pentaaza-4,5,7,9-Tetraboradihydronaphthalene	Organoboron heterocyclic compound	1.3
21	2-Bromo-4,6-Di-(Tert-Butyl-Phenol Mesylate	Substituted phenolic compound	8.07

Note: GC-MS (gas chromatography-mass spectrometry). Compound identification was based on retention time and comparison with standard library data. % area represents relative abundance and not absolute quantification.

Fourier transform infrared spectroscopy (FTIR) analysis

FTIR analysis was carried out to assess potential interactions within the constituents of the nanoemulsion. As shown in fig. 2, LO exhibited typical peaks at 1735 cm^{-1} and 1172 cm^{-1}, equivalent to C=O stretching of esters and C–O stretching of tertiary alcohols [29]. A peak at 2927 cm^{-1} indicated C–H stretching, while peaks between 1019-918 cm^{-1} were attributed to C=C bending vibrations. The spectrum of the physical mixture showed a combination of individual peaks without any significant shifts.

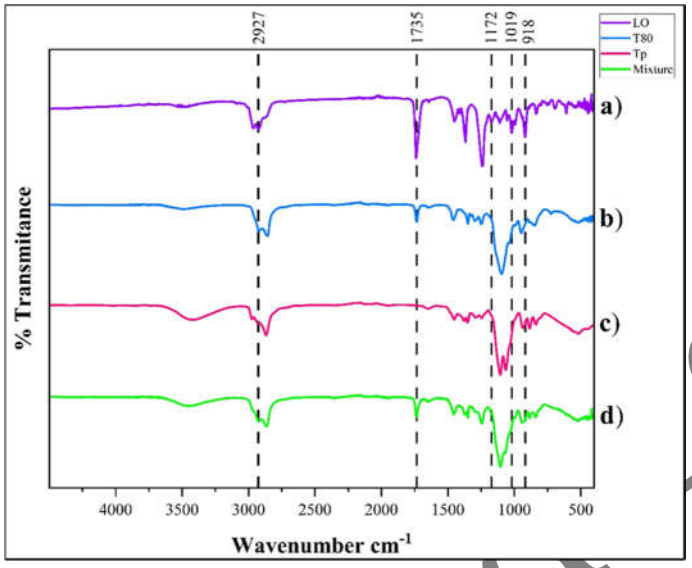

Fig. 2: FTIR graph of a) LO, b) T80, c) Tp, d) mixture of oil and s-mix indicating no chemical interactions between the mixture

Construction of pseudoternary phase plot

Pseudoternary phase plots were drawn to discover an optimums-mix system and define the nanoemulsion region. Initial trials using T80 alone resulted in unstable emulsions. Incorporation of a co-surfactant improved system stability. Among various combinations, the T80-Tp (1:2) system showed the largest nanoemulsion region. However, it exhibited phase separation after 24 h. In contrast, the 2:1 ratio, though with a slightly smaller region (fig. 3), remained stable over 24 h. Table 3 represents the amount of water required to obtain turbidity for various s-mix ratios.

Table 3: Emulsification study of T80 and Tp, indicating the amount of water required for turbidity for various s-mix ratios

Oil (ml)	S-mix (ml)	Water required for turbidity (ml)		
		S-mix (1:1)	S-mix (1:2)	S-mix (2:1)
0.1	0.9	5	5	4
0.2	0.8	4.1	1.4	4
0.3	0.7	1.2	1.3	4
0.4	0.6	0.9	1	1.8
0.5	0.5	0.6	0.7	0.9
0.6	0.4	0.4	0.6	0.4
0.7	0.3	0.4	0.4	0.4
0.8	0.2	0.4	0.4	0.6
0.9	0.1	0.4	0.7	0.7

Note: value represent volume (ml) of water required to obtain turbidity during titration.

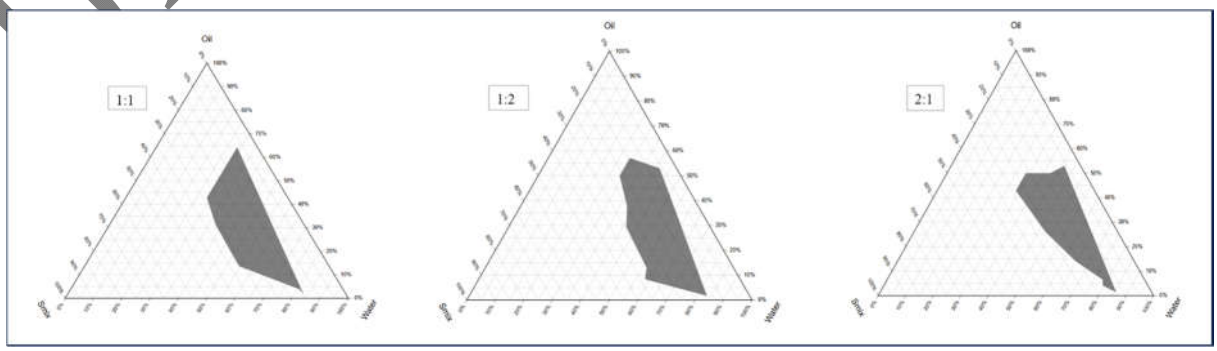

Fig. 3: Pseudoternary phase plots of s-mix, T80 and Tp in ratios 1:1, 1:2 and 2:1

Characterization of nanoemulsion

Zeta potential and particle size measurement

Table 3 summarizes the prepared nanoemulsion batches with their corresponding ZP, PS and PDI.

Table 4: ZP, PS and PDI of nanoemulsion batches

Batch	ZP (mV)	PS (nm)	PDI
A1	-10.7±2.96	87.54±2.63	0.114±0.001
A2	-6.73±2.30	132.9±3.16	0.186±0.002
A3	-9.82±0.49	75.57±0.96	0.219±0.000

Note: value are expressed as mean±SD (n = 3). ZP (zeta potential) provides an estimate of the physical stability of the formulation. PS (particle size) distribution of droplets is indicated by PDI (polydispersity index).

Thermodynamic stability of nanoemulsion

Results of thermodynamic stability for all batches are presented in table 4. Batches A1 and A2 remained stable during centrifugation and heating-cooling but showed phase separation after the freeze-thaw cycle. In contrast, batch A3 remained stable under all stress conditions (fig. 4). It exhibited desirable nanoscale properties.

Table 5: Thermodynamic stability evaluation and characterization of nanoemulsion batches

Batch	Centrifugation	Heating-cooling cycle	Freeze-thaw cycle	ZP (mV)	PS (nm)	PDI	Stability status
A1	Pass	Pass	Fail	-	-	-	Phase separation, unstable
A2	Pass	Pass	Fail	-	-	-	Phase separation, unstable
A3	Pass	Pass	Pass	-11±0.98	98.91±1.02	0.174±0.001	Stable

Note: Thermodynamic stability was assessed using centrifugation (5000 rpm, 60 min), heating-cooling cycles (4-40 °C), and freeze-thaw cycles (-25 °C to room temperature). ZP (zeta potential), PS (particle size) and PDI (polydispersity index). value are expressed as mean±SD (n = 3).

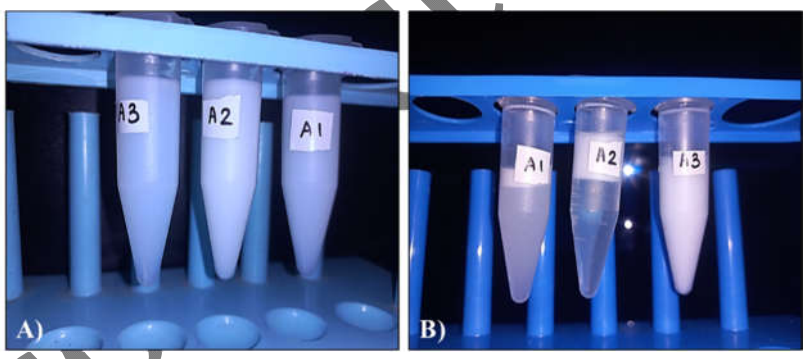

Fig. 4: Nanoemulsion batches A1, A2 and A3 A) before thermodynamic stability and B) after thermodynamic stability

Drug content

The drug content of batch A3 was determined using UV-VIS spectrophotometry at 273 nm. Batch A3 showed an average drug content of 92.3%±2.8, (mean±SD; n = 3) indicating uniform distribution.

Drug release study using the dialysis bag method

The release study was performed using a dialysis membrane (MWCO 12-14 kDa), allowing diffusion of LO across the membrane. The quantification of released drug was carried out spectrophotometrically at 278 nm using a pre-established calibration curve of LO in PBS, which showed excellent linearity (R^2 = 0.9994) (fig. 5). The quantification wavelength (278 nm) differed slightly from drug content analysis (273 nm) due to solvent-dependent shifts in absorbance between ethanol and PBS. As shown in fig. 6, batch A3 demonstrated a considerably enhanced and controlled release of 96.93%±0.48 (mean±SD; n = 3) compared to pure LO (60.35%±0.6) at 8 h. A3 showed significantly higher drug release than pure LO at 8th h (unpaired t-test, n = 3, $p<0.0001$).

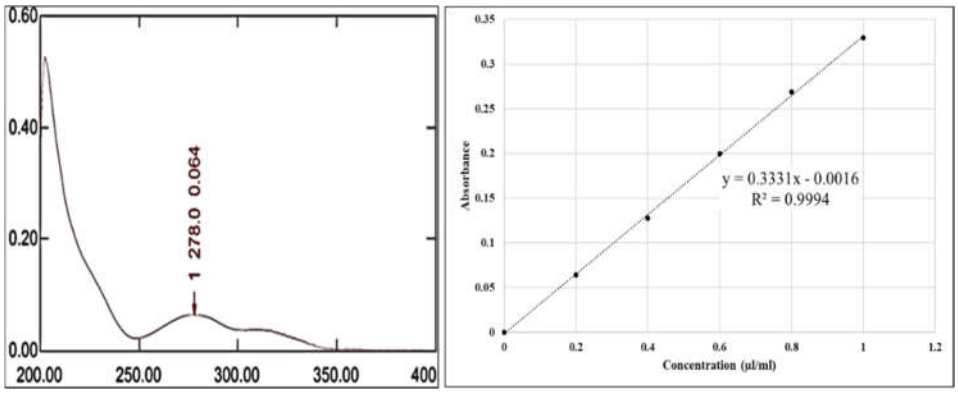

Fig. 5: UV-VIS spectra and linearity graph of pure LO in PBS 7.4

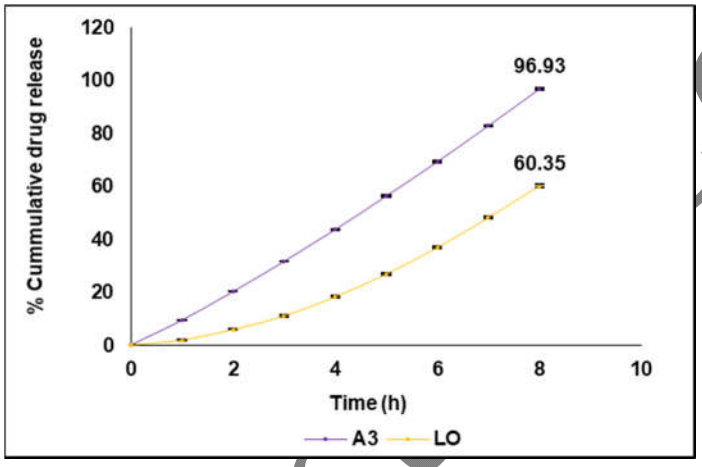

Fig. 6: *In vitro* drug release profile of pure LO and batch A3 using dialysis membrane (MWCO 12-14 kDa) in PBS pH 7.4 expressed as % cumulative release (mean±SD, n = 3). A3 exhibited significantly higher release than LO at the 8thh ($p<0.0001$, unpaired t-test with Welch's correction)

Release kinetics

The release data of batch A3 were fitted to some kinetic models, including zero order, 1storder, Higuchi matrix, Hixson-Crowell, and Korsmeyer-Peppas equations. Among these, the Korsmeyer-Peppas model showed the best fit with a correlation coefficient (R^2) of 0.9912, a release rate constant (k) of 9.5346 and a diffusional exponent (n) of 0.3399 (Equation 2), indicating a diffusion-controlled release mechanism (fig. 7).

$$F = k_{kp} \times t^{n} \ldots (2)$$

Where, F = fraction of drug released at time t, k_{kp} = rate constant for Korsmeyer-Peppas, t = time, n = diffusional exponent.

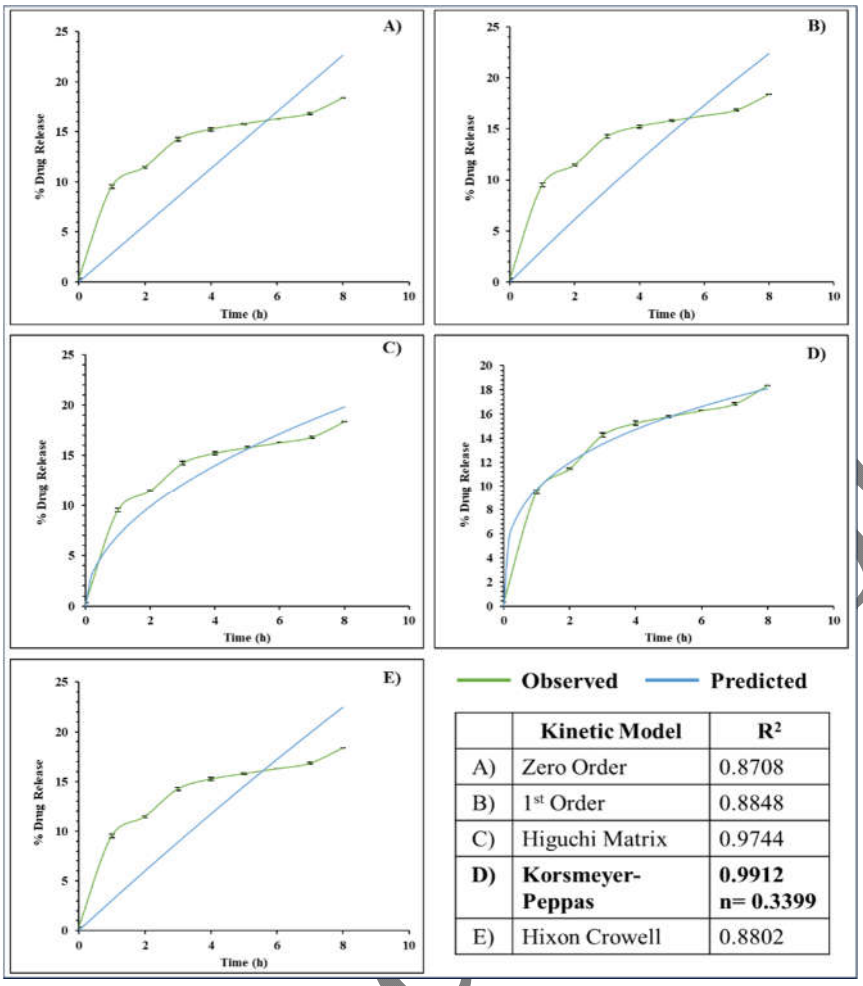

	Kinetic Model	R^2
A)	Zero Order	0.8708
B)	1st Order	0.8848
C)	Higuchi Matrix	0.9744
D)	**Korsmeyer-Peppas**	**0.9912 n= 0.3399**
E)	Hixon Crowell	0.8802

Fig. 7: Release data were fitted to multiple kinetic models A) zero order, B) 1st order, Higuchi matrix, Hixson-Crowell, and Korsmeyer-Peppas models. The Korsmeyer-Peppas model showed the best fit, with a diffusional exponent indicating fickian diffusion

***In vitro* DPPH radical scavenging assay**

The antioxidant potential of LO and the optimized nanoemulsion batch A3 was calculated by the DPPH radical scavenging assay, taking ascorbic acid as the standard reference (fig. 8). All tested samples showed a concentration-dependent increase in scavenging potential. Ascorbic acid exhibited the highest activity across all concentrations, reaching 95.59±0.42% inhibition at 0.5% (v/v). Both LO and batch A3 demonstrated moderate antioxidant potential; however, at the tested diluted concentrations (0.1-0.5% v/v), pure LO exhibited higher % scavenging activity than batch A3. At the highest tested concentration (0.5% v/v), LO and A3 showed scavenging values of 64.95±0.34% and 53.82±0.04%, respectively. Nevertheless, when the undiluted formulation (100% A3) was evaluated, batch A3 demonstrated 83.93±0.5% scavenging activity, indicating that the antioxidant potential of the nanoemulsion becomes more evident at its native concentration. All the values are expressed as mean±SD; n = 3. Significantly higher DPPH scavenging activity of LO compared to A3 at all concentrations tested was confirmed using Šídák's post-hoc test (adjusted $p<0.05$).

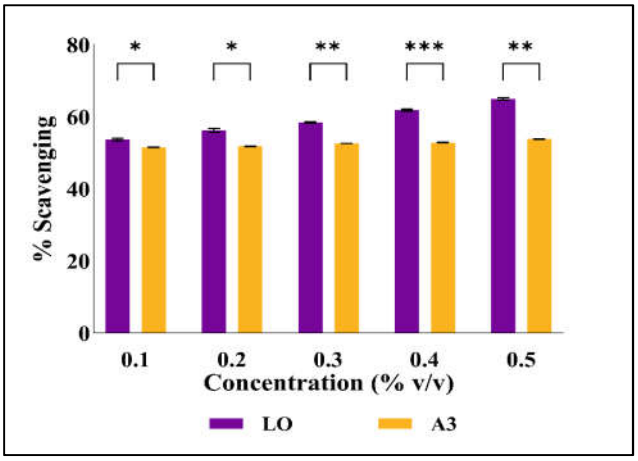

Fig. 8: DPPH radical scavenging activity of pure LO and optimized nanoemulsion (A3), with ascorbic acid as the positive control. Data are expressed as mean±SD (n = 3). Pure LO exhibited higher activity at lower dilutions, whereas the undiluted nanoemulsion demonstrated high scavenging activity. *p<0.05, **p<0.01, ***p<0.001 compared to A3 at the corresponding concentration (two-way ANOVA)

In vitro antimicrobial assay

The disc diffusion method was employed to evaluate the antimicrobial activity of batch A3 on *S. aureus* (fig. 9). The zone of inhibition of rifampicin was 28.33±0.58 mm (mean±SD; n = 3). No activity was shown by the blank. A consistent 7 mm inhibition zone at concentrations ranging from 6.25% to 100% was exhibited by batch A3 (fig. 9), indicating a weak antimicrobial response.

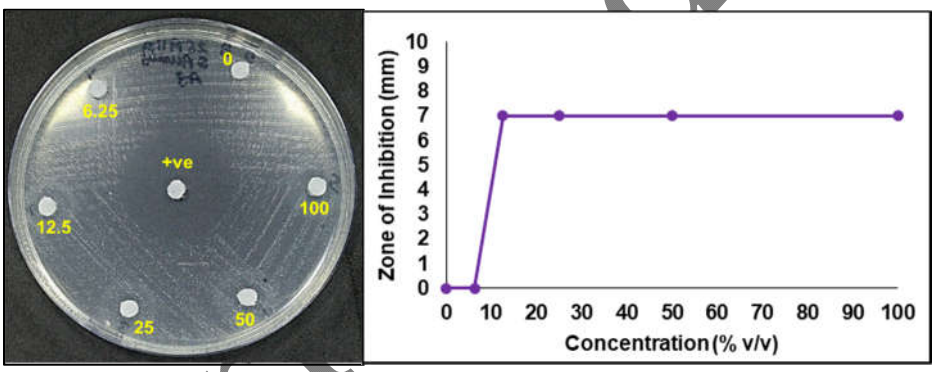

Fig. 9: Antimicrobial activity indicating zone of inhibition; rifampicin (3µg) positive control; 10 µl of batch A3 in various concentrations 0, 6.25, 12.5, 25, 50 and 100% (v/v); and antimicrobial activity of batch A3 expressed as zone of inhibition (mm) on *S. aureus*, (mean±SD, n = 3). Error bars are not shown as identical zone of inhibition values were observed across triplicate measurements**

Morphological analysis

Morphological analysis of HaCaT cells before treatment, blank nanoemulsion and after treatment with batch A3 revealed some notable structural changes, as depicted in fig. 10. Untreated cells in fig. 10A showed typical spindle-shaped morphology with intact membranes and high confluency. There was no significant change in the morphology of the cells (fig. 10B) when treated with blank nanoemulsion. While, treated cells (fig. 10C) revealed membrane blebbing, rounding and significant detachment from the surface with decreased cell density.

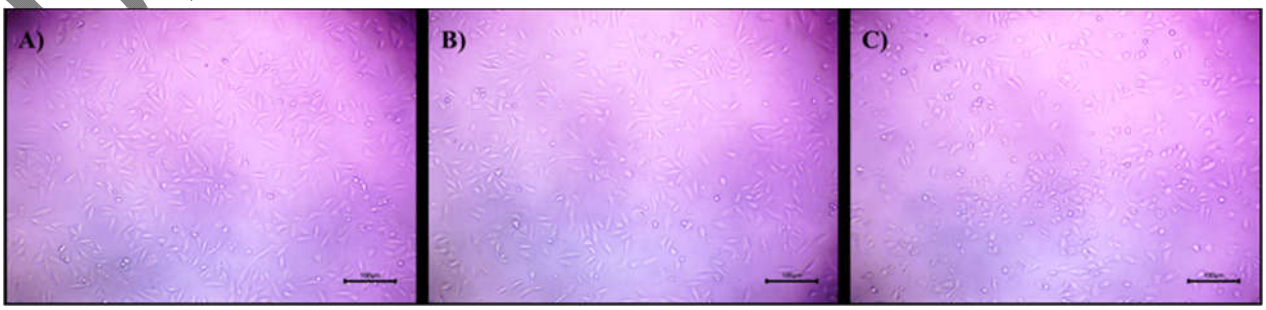

Fig. 10: Morphological analysis on stimulated HaCaT cells after 24 h treatment A) untreated control, B) blank nanoemulsion and C) batch A3, observed under 100× magnification

Cytotoxicity study

The cytotoxic potential of batch A3 was evaluated by the MTT assay. The minimal cytotoxic effect of blank nanoemulsion, as seen in morphological analysis, was confirmed by the MTT assay (fig. 11). At the highest concentration (50 µl**/ml), the percentage cell viability observed was 96.19% for the blank nanoemulsion, 10.50% for dithranol, and 5.61% for batch A3. The IC_{50} value of batch A3 (0.4198±0.047 µl**/ml) was markedly lower than that of Dithranol (7.843±0.029 µl**/ml), indicating higher cytotoxic potency. All the values are expressed as mean±SD, n = 4. Post-hoc Šídák analysis showed significantly lower viability for A3 compared to dithranol at concentrations from 0.78-25 µl**/ml (adjusted p<0.0001-0.0004), with the greatest differences at 1.56-3.125 µl**/ml. No significant difference was observed at 0 or 50 µl**/ml. Batch A3 displayed a clear dose-dependent decrease in cell viability (fig. 12).

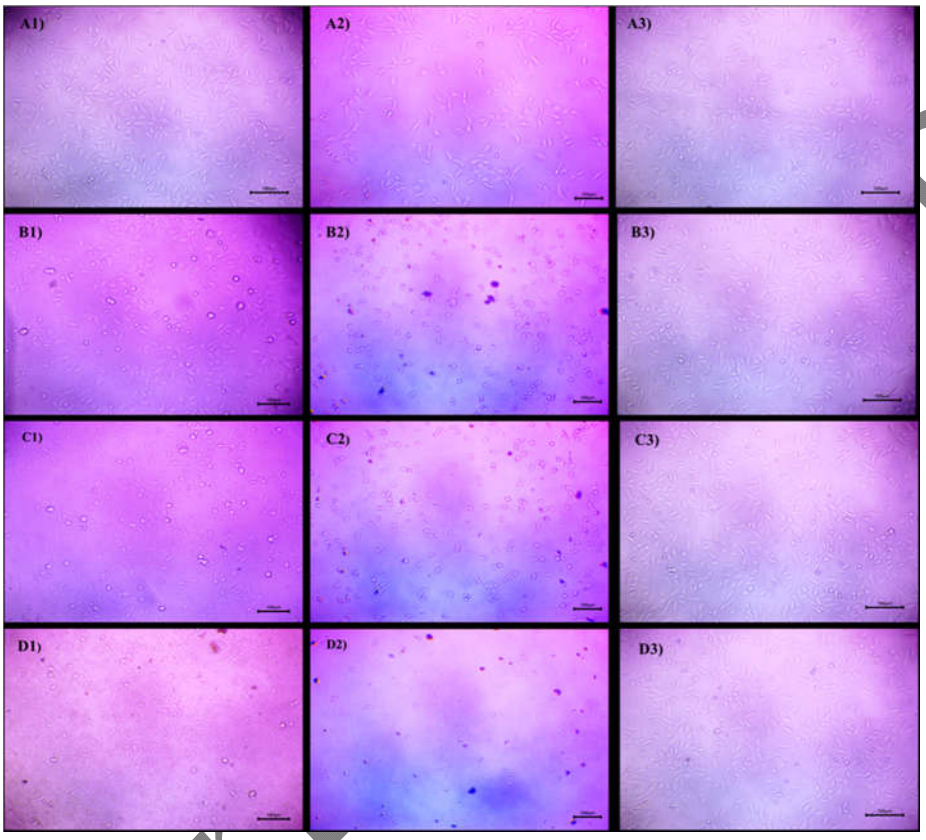

Fig. 11: Bright field microscopic images of MTT assay for standard dithranol (A1: control; B1: 0.78 µl/ml; C1: 6.25 µl**/ml; D1: 50 µl**/ml), batch A3 (A2: control; B2: 0.78 µl**/ml; C2: 6.25 µl**/ml; D2: 50 µl**/ml) and blank nanoemulsion (A3: control; B3: 0.78 µl**/ml; C3: 6.25 µl**/ml; D3: 50 µl**/ml)**

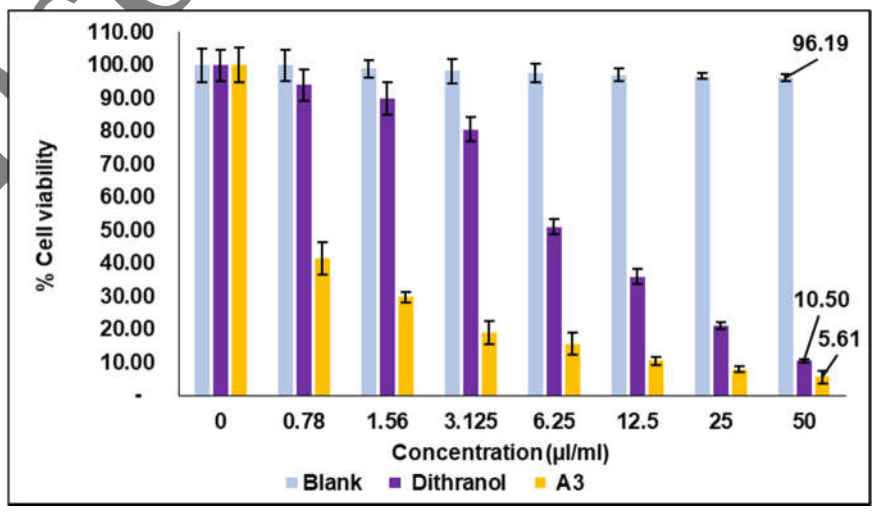

Fig. 12: Cytotoxicity of blank nanoemulsion, batch A3 and dithranol on HaCaT cells measured using the MTT assay after 24 h treatment. Results are expressed as percentage cell viability relative to untreated control (mean±SD, n = 4)

Enzyme-linked immunosorbent assay (ELISA)

An ELISA assay was carried out to quantify levels of IL-17 and IL-22 in HaCaT cells, with the control group set as baseline (100±0.33%). The blank nanoemulsion group showed minimal effect (98±0.21%) on cytokine levels compared to the untreated control. Dithranol-treated cells showed a reduced IL-17 level to 94.13±0.55%, while batch A3 treatment further decreased IL-17 expression to 90.01±1.99%. Similarly, IL-22 expression was markedly reduced following treatment, with dithranol and batch A3 lowering IL-22 levels to 62±1.38% and 71±0.27%, respectively (fig. 13). All the values are expressed as mean±SD, n = 3.

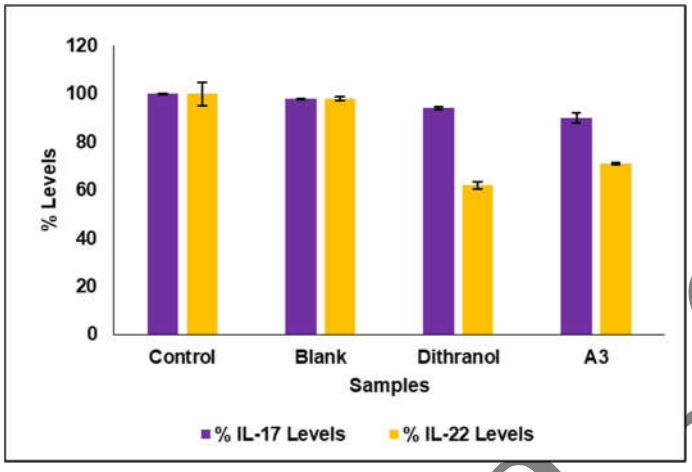

Fig. 13: Effect of blank nanoemulsion, batch A3 and dithranol on IL-17 and IL-22 levels in HaCaT cells measured using ELISA. Cytokine levels are expressed relative to the stimulated control (mean±SD, n = 3)

DISCUSSION

The constituents of LO identified by GC-MS analysis were predominantly monoterpenes and esters, with linalool (monoterpene alcohol) and linalyl acetate (ester) as the major components, which are known to contribute to the biological activity of LO [30]. Additionally, the presence of α-terpineol and isobornyl acetate synergizes its potential for dermatological uses. The presence of acetate and alcohol groups in the FTIR spectra indicates the presence of linalyl acetate and linalool, respectively. The physical mixture of LO, T80, and Tp retained its characteristic peaks without any alteration, which indicates the absence of chemical interaction among them. This suggests that there is no physical or chemical incompatibility among the components of batch A3.

The instability observed in the T80-only system in the emulsification experiment indicated the need for a co-surfactant. In the pseudoternary phase diagram, 1:2 ratio of T80-Tp showed a wider nanoemulsion region, but after 24 h, phase separation was seen, indicating instability. The 2:1 ratio was chosen as it provided higher emulsification efficiency with acceptable stability. PS analysis for all prepared batches falls within the acceptable range. ZP values, show enough electrostatic repulsion, confirming that formulations are stable at the nanoscale, suggesting their use for further studies. Batch A2 exhibited a relatively low ZP value, which may indicate limited electrostatic stabilization. However, the presence of non-ionic surfactants such as T80 and Tp can provide steric stabilization, contributing to the observed short-term stability of the formulation. Additionally, the robustness and stability of nanoemulsions are strengthened by globule analysis results. In the thermodynamic stability test, the instability of batches A1 and A2 during freeze-thaw stress specified instability for long-term storage. With a narrow PDI and sufficient ZP, which supported homogeneity and electrostatic stability, batch A3 showed consistent stability throughout tests. These characteristics support batch A3 as the stable formulation for further analysis. The obtained drug content indicated uniform distribution of LO within the nanoemulsion matrix. Accurate quantification was likely supported by the use of magnetic stirring and ethanol dilution, which improved dispersion. These findings suggest easy reproducibility of batch A3 with the currently used method.

The *in vitro* drug release showed an improved release profile for batch A3, indicating its nanosized droplet, better surface area, and the solubilizing effect of the s-mix system, which collectively allow efficient drug diffusion through the dialysis membrane. Rajitha *et al.* (2019) observed that the cumulative drug release of a methotrexate-loaded topical nanoemulsion at pH 7.4 was around 15.13% after 12 h, indicating restricted drug diffusion and poor partitioning into the aqueous phase. While, the current formulation (batch A3) demonstrated a significantly improved release pattern, reaching about 97% cumulative drug release in just 8 h. This considerable change demonstrated the higher efficiency of batch A3 in comparison to the previously reported nanoemulsion system by exhibiting superior diffusion behaviour and enhanced formulation parameters [31]. These findings support the idea that nano emulsification enhances the therapeutic potential and bioavailability of LO. Additionally, the release kinetics that best suit the Korsmeyer-Peppas model suggest a diffusion-controlled mechanism, which is generally observed in drug delivery systems based on polymeric materials and nanoemulsions [32]. While the formulation does not demonstrate prolonged sustained release over extended durations, the enhanced and relatively controlled release compared to LO may be advantageous for topical applications by ensuring improved local availability at the site of action [33]. These characteristics are highly useful for managing chronic skin disorders like psoriasis. The wavelengths of detection by UV-VIS differ in drug content and drug release, as the drug content analysis was performed in ethanol at 273 nm, whereas the release study was conducted in PBS (pH 7.4) at 278 nm. This shift in wavelength is attributed to the change in solvent system, which influences the absorbance characteristics of LO.

In the DPPH assay, the moderate radical-scavenging action of LO was indicative of phytoconstituents, including linalool, which contribute hydrogen atoms to neutralize free radicals. The encapsulation of linalool and linalyl acetate within the nanoemulsion matrix, which limits their rapid availability to interact with DPPH radicals, could be responsible for batch A3's comparatively lower activity at lower doses. However, the noticeable increase in scavenging efficiency at higher concentrations indicates that these active ingredients are released from the nanoemulsion system in a concentration-dependent manner. This suggests that nanoencapsulation retains antioxidant molecules and facilitates their controlled release,

restoring and perhaps improving their activity at larger concentrations. These findings indicate that the developed LO nanoemulsion could provide therapeutic effects against oxidative stress linked with inflammatory skin disorders such as psoriasis [34].

In the antimicrobial assay, *S. aureus* was chosen as a bacterial strain due to its clinical relevance in psoriatic skin infections. Colonization of psoriatic lesions by *S. aureus* has been widely reported to aggravate disease severity by releasing exotoxins and superantigens that promote T-helper (Th1/Th17)-mediated inflammatory cascades [35–37]. Moreover, *S. aureus* is one of the predominant g-positive pathogens involved in secondary infections of psoriatic plaques, making it a suitable indicator organism for preliminary antimicrobial screening of topical formulations [38]. The disc diffusion method was selected as a preliminary screening tool due to its simplicity, cost-effectiveness, and widespread use for the initial evaluation of antimicrobial activity, particularly in essential oil-based formulations. The consistent zone of inhibition (~7 mm) across all tested concentrations suggests that batch A3 exhibits minimal or weak antimicrobial activity under the experimental conditions [39]. This observation is likely influenced by the limited diffusion of the lipophilic components of LO through the aqueous agar medium rather than a true concentration-dependent antibacterial effect. However, this method has inherent limitations in evaluating essential oil-based formulations, and future studies employing broth dilution or MIC-based methods would provide a more reliable assessment of antimicrobial activity. Although the present study focused on *S. aureus* due to its pathophysiological significance in psoriasis, future investigations incorporating g-negative strains such as *Escherichia coli* or *Pseudomonas aeruginosa* could provide a more comprehensive antimicrobial profile of the formulation.

For morphological analysis, the HaCaT cell line was employed as the *in vitro* model in the present study owing to its well-established relevance in psoriasis research. Selection of HaCaT cells was done as they are highly adaptable and responsive to environmental conditions. Since keratinocytes are the principal effector cells involved in epidermal thickening and cytokine-driven inflammation in psoriasis, their use provides a robust and physiologically pertinent system for preliminary evaluation of anti-psoriatic activity [40, 41]. Although inclusion of additional immune-responsive cell lines such as THP-1 macrophages or fibroblasts could further delineate immuno-epidermal interactions, the HaCaT model remains the most widely accepted *in vitro* platform for initial screening of topical agents intended for psoriasis management. The cell treated with blank nanoemulsion depicted no observable change in the morphology when compared with the untreated cells. The observed morphological changes in treated HaCaT cells indicate apoptosis or necrosis. These findings suggest that the observed apoptotic effect is due to LO alone and not because of the presence of T80 or Tp. These changes reflect batch A3's cytotoxic property, indicating its ability to disrupt both the structure and viability of psoriatic keratinocytes. These findings are important for evaluating the efficacy of batch A3.

In the MTT assay, the blank nanoemulsion showed minimal cytotoxic effect, indicating the obtained cytotoxicity is purely due to the presence of LO and not the excipients. Dithranol was selected as a comparator due to its well-established topical anti-psoriatic action, particularly its direct effect on keratinocyte hyper proliferation. It acts by inhibiting keratinocyte hyperproliferation and reducing epidermal thickness through downregulation of pro-inflammatory cytokines, along with suppression of DNA synthesis, while methotrexate majorly reduces neutrophil chemotaxis and calcipotriol binds to the vitamin D receptor. Thus, the action of dithranol complements the mechanism of LO, which targets key cytokines such as IL-17, IL-22, and TNF-α, thereby limiting keratinocyte proliferation. As a topical nanoemulsion, the formulation ensures direct interaction with hyperproliferative keratinocytes [9, 42, 43]. The batch A3 had a considerably lower IC_{50} value than dithranol, indicating stronger anti-proliferative activity against psoriatic keratinocytes and potential for psoriasis treatment. At moderate doses, batch A3's higher cytotoxicity than dithranol can be due to increased cellular absorption facilitated by nanoemulsion-mediated penetration. Jain *et al.* (2017) observed that a topical nanoemulsion containing clobetasol and calcipotriol had cytotoxic action on HaCaT cells, with roughly 50% cell viability at a dose of 50 µg/ml. Similarly, Carolina *et al.* (2023) reported that treatment with a LO emulsion resulted in approximately 45% viability in HaCaT cells. In comparison, the current formulation (batch A3) displayed a substantially greater anti-proliferative effect, with just 5.61% viable cells at 50 µl**/ml. This noticeable decrease in cell viability shows improved anti-psoriatic potential of the developed LO nanoemulsion compared to previously reported topical nanoemulsion systems [44, 45]. While the Selectivity Index could not be established due to a lack of NHDF data, future research should include it to assess therapeutic safety. The observed dose-dependent cytotoxicity validates batch A3's potential as an effective and targeted anti-psoriatic formulation. While morphological alterations such as cell shrinkage and membrane blebbing signal apoptotic or necrotic processes, the current study did not include apoptosis-specific assays. Therefore, confirmation of the underlying cell death process would require specific staining methods such as DAPI, FITC-Annexin V, or TUNEL tests in future investigations.

In ELISA, the drop in IL-17 levels after exposure to batch A3 suggests a meaningful anti-inflammatory impact. Although both dithranol and batch A3 reduced IL-17 levels, batch A3 demonstrated a comparable or marginally improved reduction. Given IL-17's critical function in psoriasis, this modest decrease indicates the formulation's immunomodulatory effect. However, considering the complex cytokine network involved in psoriasis pathogenesis, this level of reduction may not be sufficient to produce a strong therapeutic outcome. These findings should therefore be interpreted as preliminary and may require further optimization or combination with other therapeutic strategies for enhanced clinical relevance. The drop in IL-22 levels after treatment with batch A3 implies that it has a modulatory influence on keratinocyte-driven inflammatory responses in psoriasis-like situations. Although both dithranol and batch A3 decreased IL-22 expression, dithranol had a stronger inhibitory impact. Since IL-22 is involved in driving keratinocyte hyperproliferation and epidermal dysregulation in psoriasis, batch A3's moderate but persistent reduction supports its potential relevance and complements the IL-17 modulation profile [46]. The blank formulation exhibited minimal effect by reduction of IL-17 and IL-22 levels to 98% compared to the stimulated control, confirming that the observed cytokine modulation is primarily attributable to LO. While the data support previously reported anti-psoriatic effects, extensive cytokine profiling is required to completely prove batch A3's immunomodulatory potential.

CONCLUSION

The present study demonstrates the successful development of a LO-based nanoemulsion with desirable physicochemical characteristics, including nanoscale droplet size, acceptable stability, and enhanced *in vitro* release compared to pure oil. The optimized formulation batch A3 exhibited notable biological activity, including moderate cytotoxic effects on HaCaT cells and measurable reductions in pro-inflammatory cytokines (IL-17 and IL-22), indicating preliminary anti-psoriatic potential. The nanoemulsion system facilitated improved dispersion and availability of active constituents, contributing to enhanced performance relative to conventional formulations. However, the observed biological effects are modest and should be interpreted as preliminary. Further studies, including *in vivo* efficacy evaluation, detailed skin permeation and retention studies, apoptosis-related assays, and selectivity assessment using normal human dermal fibroblasts, are required to establish the therapeutic relevance and safety profile of the formulation. Such investigations will be essential for advancing this system toward clinical application.

FUNDING

Nil

ABBREVIATIONS

LO: Lavender Oil, Tp: Transcutol P, T80: Tween 80, PDI: Polydispersibility Index, PS: Particle Size, ZP: Zeta Potential

AI USE STATEMENT

The author used ChatGPT for language editing and improving the clarity of the manuscript. The author reviewed and edited the output and takes full responsibility for the final content.

AUTHORS CONTRIBUTIONS

PC: Conceptualization, methodology, investigation, data curation, formal analysis, and writing-original draft preparation. SJ: Supervision, validation, data interpretation, statistical analysis, and writing, review, and editing. Both authors have read and approved the final manuscript.

CONFLICT OF INTERESTS

Declared none

REFERENCES

1. Gudjonsson JE, Elder JT. Psoriasis: epidemiology. Clin Dermatol. 2007;25(6):535-46. doi: 10.1016/j.clindermatol.2007.08.007. PMID 18021890.
2. de Rie MA, Goedkoop AY, Bos JD. Overview of psoriasis. Dermatol Ther. 2004;17(5):341-9. doi: 10.1111/j.1396-0296.2004.04037.x. PMID 15379769.
3. Yamanaka K, Yamamoto O, Honda T. Pathophysiology of psoriasis: a review. J Dermatol. 2021;48(6):722-31. doi: 10.1111/1346-8138.15913, PMID 33886133.
4. Coimbra S, Figueiredo A, Castro E, Rocha-Pereira P, Santos-Silva A. The roles of cells and cytokines in the pathogenesis of psoriasis. Int J Dermatol. 2012;51(4):389-95; quiz 395. doi: 10.1111/j.1365-4632.2011.05154.x, PMID 22435425.
5. Nograles KE, Zaba LC, Guttman-Yassky E, Fuentes-Duculan J, Suárez-Fariñas M, Cardinale I et al. Th17 cytokines interleukin (IL)-17 and IL-22 modulate distinct inflammatory and keratinocyte-response pathways. Br J Dermatol. 2008;159(5):1092-102. doi: 10.1111/j.1365-2133.2008.08769.x. PMID 18684158.
6. Zheng Y, Danilenko DM, Valdez P, Kasman I, Eastham-Anderson J, Wu J et al. Interleukin-22, a T(H)17 cytokine, mediates IL-23-induced dermal inflammation and acanthosis. Nature. 2007;445(7128):648-51. doi: 10.1038/nature05505, PMID 17187052.
7. Shruti S, Ravinder K, Gurvinder S, Saurabh S, Saurabh Singh. Psoriasis: an integrated review of a complex immune-mediated disease. Asian J Pharm Clin Res. 2026;19(1):16-24. doi: 10.22159/ajpcr.2026v19i1.57074.
8. Rahman M, Alam K, Ahmad MZ, Gupta G, Afzal M, Akhter S et al. Classical to current approach for treatment of psoriasis: a review. Endocr Metab Immune Disord Drug Targets. 2012;12(3):287-302. doi: 10.2174/187153012802002901, PMID 22463723.
9. Rai VK, Sinha P, Yadav KS, Shukla A, Saxena A, Bawankule DU et al. Anti-psoriatic effect of *Lavandula angustifolia* essential oil and its major components linalool and linalyl acetate. J Ethnopharmacol. 2020;261:113127. doi: 10.1016/j.jep.2020.113127. PMID 32623016.
10. Seo YM, Jeong SH. Effects of blending oil of lavender and thyme on oxidative stress, immunity, and skin condition in atopic dermatitis induced mice. J Korean Acad Nurs. 2015;45(3):367-77. doi: 10.4040/jkan.2015.45.3.367, PMID 26159138.
11. Cardia GF, Silva-Filho SE, Silva EL, Uchida NS, Cavalcante HA, Cassarotti LL et al. Effect of lavender (*Lavandula angustifolia*) essential oil on acute inflammatory response. Evid Based Complement Alternat Med. 2018;2018:1413940. doi: 10.1155/2018/1413940, PMID 29743918.
12. Gunaseelan S, Balupillai A, Govindasamy K, Ramasamy K, Muthusamy G, Shanmugam M et al. Linalool prevents oxidative stress activated protein kinases in single UVB-exposed human skin cells. PLOS One. 2017;12(5):e0176699. doi: 10.1371/journal.pone.0176699. PMID 28467450.
13. Moon PD, Han NR, Lee JS, Kim HM, Jeong HJ. Effects of linalyl acetate on thymic stromal lymphopoietin production in mast cells. Molecules. 2018;23(7):1711. doi: 10.3390/molecules23071711, PMID 30011850.
14. Truong S, Mudgil P. The antibacterial effectiveness of lavender essential oil against methicillin-resistant *Staphylococcus aureus*: a systematic review. Front Pharmacol. 2023;14:1306003. doi: 10.3389/fphar.2023.1306003, PMID 38130406.
15. Manzoor A, Asif M, Khalid SH, Ullah Khan I, Asghar S. Nanosizing of lavender, basil, and clove essential oils into microemulsions for enhanced antioxidant potential and antibacterial and antibiofilm activities. ACS Omega. 2023;8(43):40600-12. doi: 10.1021/acsomega.3c05394, PMID 37929152.
16. Preeti SS, Sambhakar S, Malik R, Bhatia S, Al Harrasi A, Rani C et al. Nanoemulsion: an emerging novel technology for improving the bioavailability of drugs. Scientifica (Cairo). 2023;2023:6640103. doi: 10.1155/2023/6640103, PMID 37928749.
17. Xu X, Zhang H, Chang A, Peng H, Li S, Zhang K et al. Astilbin alleviates IL-17-induced hyperproliferation and inflammation in HaCaT cells via inhibiting ferroptosis through the cGAS-STING pathway. Int J Mol Sci. 2025;26(11):5075. doi: 10.3390/ijms26115075, PMID 40507886.
18. Gedikoğlu A, Öztürk Hİ, Özçoban A. Analysis of the chemical composition, antimicrobial, and antioxidant qualities of microwave and supercritical CO_2-extracted lavender essential oils cultivated in a hyperarid region of türkiye. Molecules. 2024;29(23):5605. doi: 10.3390/molecules29235605, PMID 39683763.
19. Barakat N. Formulation design of indomethacin-loaded nanoemulsion for transdermal delivery. Pharm Anal Acta. 2011;s2:s2. doi: 10.4172/2153-2435.S2-002.
20. Jagdale S, Chaudhari B. Optimization of microemulsion based transdermal gel of triamcinolone. Recent Pat Anti-infect Drug Discov. 2017;12(1):61-78. doi: 10.2174/1574891X12666170426092911, PMID 28506203.
21. Bodke V, Kumbhar P, Belwalkar S, Mali AS, Waghmare K. Design and development of nanoemulsion of *Smilax china* for anti-psoriasis activity. Int J Pharm Pharm Sci. 2024;16(5):54-66. doi: 10.22159/ijpps.2024v16i5.50327.
22. Gurpreet K, S. K. Singh. Review of nanoemulsion formulation and characterization techniques. Indian J Pharm Sci. 2018;80(5):781-9. doi: 10.4172/pharmaceutical-sciences.1000422.
23. Laxmi M, Bhardwaj A, Mehta S, Mehta A. Development and characterization of nanoemulsion as carrier for the enhancement of bioavailability of artemether. Artif Cells Nanomed Biotechnol. 2015;43(5):334-44. doi: 10.3109/21691401.2014.887018, PMID 24641773.
24. Hable AA, Jagdale SC, Chabukswar AR. Selection of optimum method for nanoparticles in lung cancer therapeutics. Biosci Biotechnol Res Asia. 2022;19(2):321-31. doi: 10.13005/bbra/2987.
25. Amin N, Das B. A review on formulation and characterization of nanoemulsion. Int J Curr Pharm Res. 2019;11(4):1-5. doi: 10.22159/ijcpr.2019v11i4.34925.
26. Danh LT, Han LN, Triet ND, Zhao J, Mammucari R, Foster N. Comparison of chemical composition, antioxidant and antimicrobial activity of lavender (*Lavandula angustifolia L.*) Essential oils extracted by supercritical CO_2, hexane and hydrodistillation. Food Bioprocess Technol. 2012;6(12):3481-9. doi: 10.1007/s11947-012-1026-z.
27. Gayatri M, Sudha U, Shubha J, Kavya K. Evaluation of antibacterial activity of *Lavandula stoechas L.* essential oil. J Spices Aromat. 2013;22(2):188-93.
28. Miastkowska M, Kantyka T, Bielecka E, Kałucka U, Kamińska M, Kucharska M, et al. Enhanced biological activity of a novel preparation of *Lavandula angustifolia* essential oil. Molecules. 2021;26(9):2458. doi: 10.3390/molecules26092458, PMID 33922508.

29. Agatonovic-Kustrin S, Ristivojevic P, Gegechkori V, Litvinova TM, Morton DW. Essential oil quality and purity evaluation via FT-IR spectroscopy and pattern recognition techniques. Appl Sci. 2020;10(20):7294. doi: 10.3390/app10207294.
30. Patil H, Waghmare J. Lavender oil: a comprehensive review of composition and applications. Asian J Res Chem. 2024;17(6):377-86. doi: 10.52711/0974-4150.2024.00063.
31. Rajitha P, Shammika P, Aiswarya S, Gopikrishnan A, Jayakumar R, Sabitha M. Chaulmoogra oil based methotrexate loaded topical nanoemulsion for the treatment of psoriasis. J Drug Deliv Sci Technol. 2019;49:463-76. doi: 10.1016/j.jddst.2018.12.020. jddst.2018.12.020.
32. Mady OY, Donia AA. A new mathematic method for calculation of Peppas-Sahlin model constants and interpret the results in relation to zero order, Higuchi, Korsmeyer-Peppas models and microcapsule structure image. World J Pharm Res. 2015;4(8):2199-246.
33. Hoffman A. Pharmacodynamic aspects of sustained release preparations. Adv Drug Deliv Rev. 1998;33(3):185-99. doi: 10.1016/s0169-409x(98)00027-1, PMID 10837659.
34. Sharma S, Cheng SF, Bhattacharya B, Chakkaravarthi S. Efficacy of free and encapsulated natural antioxidants in oxidative stability of edible oil: special emphasis on nanoemulsion-based encapsulation. Trends Food Sci Technol. 2019;91:305-18. doi: 10.1016/j.tifs.2019.07.030. tifs.2019.07.030.
35. Totté JE, van der Feltz WT, Bode LG, van Belkum A, van Zuuren EJ, Pasmans SG. A systematic review and meta-analysis on *Staphylococcus aureus* carriage in psoriasis, acne and rosacea. Eur J Clin Microbiol Infect Dis. 2016;35(7):1069-77. doi: 10.1007/s10096-016-2647-3, PMID 27151386.
36. Ng CY, Huang YH, Chu CF, Wu TC, Liu SH. Risks for *Staphylococcus aureus* colonization in patients with psoriasis: a systematic review and meta-analysis. Br J Dermatol. 2017;177(4):967-77. doi: 10.1111/bjd.15366, PMID 28160277.
37. Balci DD, Duran N, Ozer B, Gunesacar R, Onlen Y, Yenin JZ. High prevalence of *Staphylococcus aureus* cultivation and superantigen production in patients with psoriasis. Eur J Dermatol. 2009;19(3):238-42. doi: 10.1684/ejd.2009.0663, PMID 19286488.
38. Patrascu IV. Chicken immunological active protein (CIAP). The immunoVIP (IVIP)group of products from an integrated perspective: applicative research, transfer of technology, productions, clinical use [abstract]. J Infect Dis Ther. 2018;6:69-70. doi: 10.4172/2332-0877-C6-053.
39. Rota C, Carramiñana JJ, Burillo J, Herrera A. *In vitro* antimicrobial activity of essential oils from aromatic plants against selected foodborne pathogens. J Food Prot. 2004;67(6):1252-6. doi: 10.4315/0362-028x-67.6.1252, PMID 15222560.
40. Váradi J, Oláh B, Hosszú D, Fenyvesi F, Remenyik J, Homoki J et al. Development of imiquimod-induced HaCaT-THP-1 co-culture for modeling of psoriasis. Eur J Pharm Sci. 2024;200:106846. doi: 10.1016/j.ejps.2024.106846. PMID 38972610.
41. Zampetti A, Mastrofrancesco A, Flori E, Maresca V, Picardo M, Amerio P et al. Proinflammatory cytokine production in HaCaT cells treated by eosin: implications for the topical treatment of psoriasis. Int J Immunopathol Pharmacol. 2009;22(4):1067-75. doi: 10.1177/039463200902200423, PMID 20074471.
42. Hollywood KA, Winder CL, Dunn WB, Xu Y, Broadhurst D, Griffiths CE et al. Exploring the mode of action of dithranol therapy for psoriasis: a metabolomic analysis using HaCaT cells. Mol Biosyst. 2015;11(8):2198-209. doi: 10.1039/c4mb00739e, PMID 26018604.
43. Kumar P, Namdev S, Rajpoot R, Kumar Savita DK. Formulation and evaluation of dithranol ethosomes for psoriasis. IJRPAS. 2025;4(9):42-53. doi: 10.71431/ijrpas.2025.4905.
44. Kaur A, Katiyar SS, Kushwah V, Jain S. Nanoemulsion loaded gel for topical co-delivery of clobitasol propionate and calcipotriol in psoriasis. Nanomedicine. 2017;13(4):1473-82. doi: 10.1016/j.nano.2017.02.009. PMID 28259803.
45. Jaramillo V, Díaz E, Muñoz LN, González-Barrios AF, Rodríguez-Cortina J, Cruz JC et al. Enhancing wound healing: a novel topical emulsion combining CW49 peptide and lavender essential oil for accelerated regeneration and antibacterial protection. Pharmaceutics. 2023;15(6):1739. doi: 10.3390/pharmaceutics15061739, PMID 37376187.
46. Zhuang L, Ma W, Yan J, Zhong H. Evaluation of the effects of IL-22 on the proliferation and differentiation of keratinocytes *in vitro*. Mol Med Rep. 2020;22(4):2715-22. doi: 10.3892/mmr.2020.11348, PMID 32945375.